Quantum Monte Carlo calculation of the equation of state of neutron matter

S. Gandolfi[*] and A. Yu. Illarionov[†]
International School for Advanced Studies, SISSA Via Beirut 2/4 I-34014 Trieste, Italy and INFN, Sezione di Trieste, Trieste, Italy

K. E. Schmidt[‡]
Department of Physics, Arizona State University, Tempe, Arizona 85287, USA

F. Pederiva[§]
Dipartimento di Fisica dell'Universitá di Trento, via Sommarive 14, I-38050 Povo, Trento, Italy and INFN, Gruppo Collegato di Trento, Trento, Italy

S. Fantoni[‖]
International School for Advanced Studies, SISSA Via Beirut 2/4 I-34014 Trieste, Italy INFN, Sezione di Trieste, Trieste, Italy and INFM DEMOCRITOS National Simulation Center, Via Beirut 2/4 I-34014 Trieste, Italy

(Received 16 March 2009; published 18 May 2009)

We calculated the equation of state of neutron matter at zero temperature by means of the auxiliary field diffusion Monte Carlo (AFDMC) method combined with a fixed-phase approximation. The calculation of the energy was carried out by simulating up to 114 neutrons in a periodic box. Special attention was given to reducing finite-size effects at the energy evaluation by adding to the interaction the effect due to the truncation of the simulation box, and by performing several simulations using different numbers of neutrons. The finite-size effects due to kinetic energy were also checked by employing the twist-averaged boundary conditions. We considered a realistic nuclear Hamiltonian containing modern two- and three-body interactions of the Argonne and Urbana family. The equation of state can be used to compare and calibrate other many-body calculations and to predict properties of neutron stars.

DOI: 10.1103/PhysRevC.79.054005 PACS number(s): 21.65.Cd, 21.65.Mn, 26.60.Kp, 24.10.Cn

I. INTRODUCTION

The equation of state of nuclear matter and its properties plays a central role in the modeling of neutron stars [1]. The density in the star ranges from a small fraction of the nuclear saturation density, $\rho_0 = 0.16$ fm^{-3}, to several times its value, which is found in the center of heavy nuclei. At such extreme conditions, no phenomenological data determined from experiments are available, and because the matter inside a neutron star is closer to neutron matter than to symmetric nuclear matter, heavy-ion collision experiments do not substantially constrain the equation of state [2]. A realistic calculation of the equation of state of neutron matter is then particularly challenging in both many-body nuclear physics and astrophysics.

The equation of state of neutron matter can in principle be computed in the framework of many-body theories using a bare interaction. A common alternative is represented by effective Skyrme forces. However, the resulting equation of state strongly depends on the parameters of the effective interaction used, even in the low-density regime [3]. At present, there are a wide range and type of Skyrme interactions. However, their nonrealistic character impairs their ability to reliably calculate the properties of neutron stars [4]. More accurate many-body techniques are then needed to perform predictive calculations.

A microscopic calculation of neutron matter starting from a nonrelativistic nucleon-nucleon and three-nucleon interaction is both challenging and of great relevance. Variational techniques based on correlated basis functions are good candidates for solving for the ground state of neutron matter. The operatorial structure of the nuclear Hamiltonian and the strong correlations induced by the high density make these techniques hard to use. The energy evaluation using the correlated basis function theory is usually performed by solving the Fermi hyper-netted chain (FHNC) equations [5] neglecting many elementary diagrams. In addition, the operatorial structure of the Hamiltonian leads to additional approximations, such as the single operator chain (SOC) approximation, because of the noncommutativity of the terms entering in the variational wave function. Therefore the resulting equation of state contains, in principle, uncontrolled approximations which may be partially corrected by computing the energy exactly up to a few first orders in the cluster expansion [6].

Despite the progress of the last several years in the determination of sophisticated two- and three-nucleon interactions, large discrepancies among different calculations of nuclear and neutron matter are still present. Quantum Monte Carlo techniques based on projection can be very accurate for calculating the ground state and low-lying excited states of nuclei. In particular, the Green's function Monte Carlo (GFMC) method was employed to fit the three-nucleon

[*]gandolfi@sissa.it
[†]illario@sissa.it
[‡]kevin.schmidt@asu.edu
[§]pederiva@science.unitn.it
[‖]fantoni@sissa.it

interaction form in nuclei up to $A = 8$ [7] and then used to test the nuclear Hamiltonian up to the ^{12}C ground state [8]. At present, the huge number of required numeric operations limits the applicability of this method to only about 14 neutrons [9].

The auxiliary field diffusion Monte Carlo (AFDMC) technique [10] combined with a fixed-phase approximation was employed to predict properties of nuclei in very good agreement with the GFMC [11] and stressed the important limitations of other many-body theories used in nuclear matter calculations [12].

In this work, we present an accurate evaluation of the equation of state of neutron matter using realistic two- and three-nucleon interactions (the Argonne v_8' and Argonne v_{18} combined with Urbana-IX [13]). The computed equation of state can be used as a benchmark for other many-body techniques.

The plan of the paper is the following. In the next section, we describe the structure of the nuclear Hamiltonian we used; in Sec. III, we briefly review the AFDMC method and explain the fixed-phase approximation. The results are presented in Sec. IV, and some conclusions are given in the last section.

II. HAMILTONIAN

Properties of a generic nuclear system can be studied starting from the nonrelativistic Hamiltonian

$$H = -\frac{\hbar^2}{2m}\sum_i \nabla_i^2 + \sum_{i<j} v_{ij} + \sum_{i<j<k} V_{ijk}, \tag{1}$$

which includes the kinetic energy operator, a two-nucleon interaction v_{ij}, and a three-nucleon interaction V_{ijk}.

The nucleon-nucleon interactions are usually dependent on the relative spin and isospin states of the nucleons and therefore written as a sum of several operators. The coefficients and radial functions that multiply each operator are adjusted by fitting experimental scattering data, and the type and number of these operators depends on the interaction. A large amount of empirical information about the nucleon-nucleon scattering problem has been accumulated. In 1993, the Nijmegen group analyzed all nucleon-nucleon scattering data below 350 MeV published in physics journals between 1955 and 1992 [14]. Nucleon-nucleon interaction models that fit the Nijmegen database with a $\chi^2/N_{\rm data} \sim 1$ are called "modern" and include the Nijmegen models [15] (Nijm93, Nijm I, Nijm II, and Reid-93), the Argonne models [16,17], and the CD-Bonn [18]. However, all of these interactions, when used alone, underestimate the triton binding energy, suggesting that the contribution of a three-nucleon force is essential to reproducing the physics of nuclei.

The most sophisticated Argonne interaction is the Argonne v_{18} [16] potential, written as a sum of 18 operators. However, we often consider another interaction, the Argonne v_8' [17] that is a simplified version of Argonne v_{18}; it contains only eight operators, and the prime symbol indicates that such potential is not just a simple truncation of Argonne v_{18} but also a reprojection, which preserves the isoscalar part in all S and P partial waves as well as in the $^3D_1$ wave and its coupling to $^3S_1$. The Argonne v_8' is a bit more attractive than Argonne v_{18} in light nuclei by about 0.5 MeV per nucleon [13], but its contribution is very similar to Argonne v_{18} in neutron drops, where the difference is about 0.06 MeV per neutron [7].

The Argonne potential between two nucleons i and j is written in the coordinate space as a sum of operators

$$v_{ij} = \sum_{p=1}^{n} v_p(r_{ij}) O_{ij}^p, \tag{2}$$

where n is the number of operators, which depends on the potential, $v_p(r)$ are radial functions, and r_{ij} is the interparticle distance.

The eight operators included in Argonne v_8' give the largest contributions to the nucleon-nucleon interaction. The first six of them come from the one-meson exchange between nucleons, while the last two terms depend on the velocity of nucleons and give the spin-orbit contribution. These eight operators are

$$O_{ij}^{p=1,8} = (1, \boldsymbol{\sigma}_i \cdot \boldsymbol{\sigma}_j, S_{ij}, \boldsymbol{L}_{ij} \cdot \boldsymbol{S}_{ij}) \times (1, \boldsymbol{\tau}_i \cdot \boldsymbol{\tau}_j), \tag{3}$$

where S_{ij} is the tensor operator

$$S_{ij} = 3(\boldsymbol{\sigma}_i \cdot \hat{r}_{ij})(\boldsymbol{\sigma}_j \cdot \hat{r}_{ij}) - \boldsymbol{\sigma}_i \cdot \boldsymbol{\sigma}_j, \tag{4}$$

$\boldsymbol{L}_{ij}$ is the relative angular momentum of couple ij

$$\boldsymbol{L}_{ij} = \frac{1}{2i}(\boldsymbol{r}_i - \boldsymbol{r}_j) \times (\boldsymbol{\nabla}_i - \boldsymbol{\nabla}_j), \tag{5}$$

and $\boldsymbol{S}_{ij}$ is the total spin of the pair

$$\boldsymbol{S}_{ij} = \tfrac{1}{2}(\boldsymbol{\sigma}_i + \boldsymbol{\sigma}_j), \tag{6}$$

with both $\boldsymbol{L}_{ij}$ and $\boldsymbol{S}_{ij}$ divided by $\hbar$ to make them unitless.

In modern interactions, these eight operators are the standard ones required to fit S- and P-wave scattering data in both triplet and singlet isospin states.

The three-nucleon interaction contribution is mainly attributed to the possible Δ intermediate states that an excited nucleon could assume after and before exchanging a pion with other nucleons. This process can be written as an effective three-nucleon interaction, and its parameters are fit to light nuclei [7,19] and eventually to properties of nuclear matter, such as the empirical equilibrium density and the energy at saturation [20]. The three-nucleon interaction must accompany the two-nucleon interaction and the total Hamiltonian studied.

The Urbana-IX three-nucleon interaction used in our calculation has the form

$$V_{ijk} = V_{2\pi} + V_R. \tag{7}$$

The Fujita-Miyazawa term [21] is spin-isospin dependent:

$$V_{2\pi} = A_{2\pi} \sum_{cyc} \Big[\{X_{ij}, X_{jk}\{\tau_i \cdot \tau_j, \tau_j \cdot \tau_k\} + \frac{1}{4}[X_{ij}, X_{jk}][\tau_i \cdot \tau_j, \tau_j \cdot \tau_k] \Big], \tag{8}$$

where

$$X_{ij} = Y(m_\pi r_{ij})\boldsymbol{\sigma}_i \cdot \boldsymbol{\sigma}_j + T(m_\pi r_{ij})S_{ij},$$
$$Y(x) = \frac{e^{-x}}{x}\xi_Y(r),$$

$$T(x) = \left(1 + \frac{3}{x} + \frac{3}{x^2}\right) Y(x)\xi_T(r),$$
$$\xi_Y(r) = \xi_T(r) = 1 - e^{-cr^2}. \quad (9)$$

The phenomenological V_R part is

$$V_{ijk}^R = U_0 \sum_{cyc} T^2(m_\pi r_{ij}) T^2(m_\pi r_{jk}). \quad (10)$$

For neutrons, the commutator terms in Eq. (8) are zero, and each of the anticommutator terms has only spin operators for two of the three neutrons.

The $A_{2\pi}$ term of Urbana-IX was originally fitted, along with the Argonne v_{18} parameters, to reproduce the triton and α particle binding energy, while the U_0 strength was adjusted to obtain the empirical equilibrium density of nuclear matter [22]. However, while the ground state of light nuclei can be exactly solved with few-body techniques, the determination of the equation of state of symmetric nuclear matter can be evaluated only using many-body techniques that contain uncontrolled approximations.

III. METHOD

A. Diffusion Monte Carlo

The auxiliary field diffusion Monte Carlo method is an extension of the usual diffusion Monte Carlo to deal with Hamiltonians that are spin-isospin dependent. The diffusion Monte Carlo method [23,24] projects out the ground-state properties by starting from a trial wave function not orthogonal to the true ground state.

Consider a generic trial wave function ψ_T expanded over a set $\{\phi_n\}$ of eigenstates of the Hamiltonian:

$$\psi_T(\mathbf{R}) = \psi(R, 0) = \sum_n c_n \phi_n(\mathbf{R}). \quad (11)$$

The propagation in imaginary time τ is given by

$$\psi(\mathbf{R}, \tau) = \sum_n c_n e^{-(H-E_0)\tau} \phi_n(\mathbf{R}), \quad (12)$$

where E_0 is a normalization factor, and $\mathbf{R}$ represent the spatial coordinates of the system. In the limit $\tau \to \infty$, $\psi(\mathbf{R}, \tau)$ approaches the lowest eigenstate ϕ_0 with the same symmetry as ψ. The evolution can be done by solving the integral equation

$$\psi(\mathbf{R}, \tau) = \int G(\mathbf{R}, \mathbf{R}', \tau)\psi(\mathbf{R}', 0) d\mathbf{R}', \quad (13)$$

where the wave function is described with a set of N_w configurations called "walkers" as follows:

$$\langle \mathbf{R}|\psi\rangle = \psi(\mathbf{R}) \cong \sum_{k=1}^{N_w} \langle \mathbf{R}|\mathbf{R}_k\rangle\langle \mathbf{R}_k|\psi\rangle \quad (14)$$

and

$$\langle \mathbf{R}|\mathbf{R}_k\rangle = \delta(\mathbf{R} - \mathbf{R}_k). \quad (15)$$

The kernel $G(\mathbf{R}, \mathbf{R}', \tau)$ is the Green's function of the system and can be expressed as the matrix element

$$G(\mathbf{R}, \mathbf{R}', \tau) = \langle \mathbf{R}|e^{-(H-E_0)\tau}|\mathbf{R}'\rangle. \quad (16)$$

By considering a generic Hamiltonian and the Trotter decomposition, the form of the Green's function in the small imaginary time-step limit $\Delta\tau \to 0$ is

$$G(\mathbf{R}, \mathbf{R}', \Delta\tau) \approx \exp\left[-\frac{V(\mathbf{R}) + V(\mathbf{R}')}{2}\Delta\tau\right] G_0(\mathbf{R}, \mathbf{R}', \Delta\tau), \quad (17)$$

where G_0 is the Green's function of the noninteracting system

$$G_0(\mathbf{R}, \mathbf{R}', \tau) = \left(\frac{m}{2\pi\hbar^2\tau}\right)^{\frac{3A}{2}} \exp\left[-\frac{m|\mathbf{R} - \mathbf{R}'|^2}{2\hbar^2\tau}\right], \quad (18)$$

and the factor due to the interaction plus the trial eigenvalue E_T is the normalization of the Green's function factor computed over the time interval τ:

$$w = \exp\left[-\left(\frac{V(\mathbf{R}) + V(\mathbf{R}')}{2} - E_T\right)\Delta\tau\right]. \quad (19)$$

The integral of Eq. (13) can be solved in a Monte Carlo way. At each time-step, all walkers are moved with the diffusion term of the free Green's function G_0, so that for each walker, a new set $\mathbf{R}'$ of spatial coordinates are generated according to

$$\mathbf{R}' = \mathbf{R} + \boldsymbol{\eta}, \quad (20)$$

where $\mathbf{R}$ is the old configuration, and $\boldsymbol{\eta}$ is a vector of random numbers with probability density G_0.

The normalization of Eq. (19), translated into a weight of the walker, is sampled using the *branching* technique in which w gives the probability of a configuration to multiply at the next step. Computationally, this is implemented by weighting estimators according to w, and generating from each single walker a number of replicas

$$n = [w + \xi], \quad (21)$$

where $\xi \in [0; 1]$ is a random number and $[x]$ means the integer part of x.

The infinite imaginary-time limit is reached by iterating this process for a sufficient total time $\tau = n\Delta\tau$.

B. Auxiliary field diffusion Monte Carlo

In nuclear Hamiltonians, the potential contains quadratic spin and isospin and tensor operators, so the many-body wave function cannot be written as a product of single-particle spin-isospin states.

For instance, let us consider the generic quadratic spin operator $\boldsymbol{\sigma}_i \cdot \boldsymbol{\sigma}_j$ where the $\boldsymbol{\sigma}$ are Pauli's matrices operating on particles. It is possible to write

$$\boldsymbol{\sigma}_i \cdot \boldsymbol{\sigma}_j = 2P_{ij}^\sigma - 1, \quad (22)$$

where P_{ij}^σ interchanges two spins, and this means that the wave function of each spin-pair must contain both components in the triplet and singlet spin state [25,26]. By considering all possible nucleon pairs in the systems, the number of possible spin states grows exponentially with the number of nucleons.

Thus, to perform a diffusion Monte Carlo calculation with standard nuclear Hamiltonians, it is necessary to sum over all the possible single-particle spin-isospin states of the system to build the trial wave function used for propagation. This is the standard approach in GFMC calculations for nuclear systems.

The idea of AFDMC is to rewrite Green's function in order to change the quadratic dependence on spin and isospin operators to a linear dependence by using the Hubbard-Stratonovich transformation.

For neutrons $\boldsymbol{\tau}_i \cdot \boldsymbol{\tau}_j = 1$, so that the isoscalar-spin operators of the Hamiltonian can be recast in a more convenient form,

$$V = \sum_{i<j} \sum_{p=1}^{6} v_p(r_{ij}) O^{(p)}(i,j) V_{\rm SI} + V_{\rm SD} = V_{\rm SI} + \frac{1}{2} \sum_{i\alpha,j\beta} \sigma_{i\alpha} A^{(\sigma)}_{i\alpha,j\beta} \sigma_{j\beta}, \tag{23}$$

where Latin indices label nucleons, Greek indices label Cartesian components, and

$$V_{\rm SI} = \sum_{i<j} [v_1(r_{ij}) + v_2(r_{ij})], \tag{24}$$

is the spin-isospin independent part of the interaction. The $3A$ by $3A$ matrix $A^{(\sigma)}$ contains the interaction between nucleons of other terms:

$$A^{(\sigma)}_{i\alpha,j\beta} = [v_3(r_{ij}) + v_4(r_{ij})]\delta_{\alpha\beta} + [v_5(r_{ij}) + v_6(r_{ij})]\left(3\hat{r}^{\alpha}_{ij}\hat{r}^{\beta}_{ij} - \delta_{\alpha\beta}\right). \tag{25}$$

The matrix A is zero along the diagonal (when $i = j$), to avoid self-interaction, and is real and symmetric, with real eigenvalues and eigenvectors given by

$$\sum_{j\beta} A^{(\sigma)}_{i\alpha,j\beta} \psi^{(\sigma)}_{n,j\beta} = \lambda^{(\sigma)}_n \psi^{(\sigma)}_{n,i\alpha}. \tag{26}$$

The matrix $A^{(\sigma)}$ has $n = 1, \ldots, 3A$ eigenvalues and eigenvectors. We can then define a new set of operators written in terms of eigenvectors of the matrix A:

$$O^{(\sigma)}_n = \sum_{j\beta} \sigma_{j\beta} \psi^{(\sigma)}_{n,j\beta}. \tag{27}$$

The spin-dependent part of Eq. (23) becomes

$$V_{\rm SD} = \frac{1}{2} \sum_{n=1}^{3A} O^{(\sigma)2}_n \lambda^{(\sigma)}_n, \tag{28}$$

and the corresponding propagator is then

$$\exp\left[-\frac{1}{2} \sum_n O^{(\sigma)2}_n \lambda^{(\sigma)}_n \Delta\tau\right]. \tag{29}$$

At first order in $\Delta\tau$, this is equivalent to

$$\prod_n \exp\left[-\frac{1}{2} O^{(\sigma)2}_n \lambda^{(\sigma)}_n \Delta\tau\right]. \tag{30}$$

Each factor can be linearized with respect to the operators O by using the Hubbard-Stratonovich transformation

$$\exp\left[-\frac{1}{2}\lambda\hat{O}^2\right] = \frac{1}{\sqrt{2\pi}} \int_{-\infty}^{\infty} dx \, \exp\left[-\frac{x^2}{2} + \sqrt{-\lambda} x \hat{O}\right]. \tag{31}$$

Green's function then becomes

$$G(\mathbf{R}, \mathbf{R}', \Delta\tau) = \left(\frac{m}{2\pi\hbar^2\Delta\tau}\right)^{\frac{3A}{2}} \exp\left[-\frac{m|\mathbf{R}-\mathbf{R}'|^2}{2\hbar^2\Delta\tau}\right] \exp\left[-V_{\rm SI}(\mathbf{R})\Delta\tau\right] \times \prod_{n=1}^{3A} \frac{1}{\sqrt{2\pi}} \int dx_n \exp\left[-\frac{x_n^2}{2}\right] \exp[\sqrt{-\lambda_n\Delta\tau} x_n O_n]. \tag{32}$$

The newly introduced variables x_n, called "auxiliary fields," are sampled to evaluate the integral of Eq. (32). For a spin state given by a product of single-particle spin functions, the linearized Green's function has the effect of changing the spin state by independently rotating the spin of each single nucleon.

The sampling of auxiliary fields to perform the integral of Eq. (31) eventually gives the same effect as the propagator with quadratic spin operators acting on a trial wave function containing all the possible good spin states. The effect of the Hubbard-Stratonovich is then to reduce the dependence of the number of operations needed to evaluate the trial wave function from exponential to linear in the number of nucleons. The price to pay is the additional computational cost due to the diagonalization of A matrices and the sampling of the integral over auxiliary fields.

Sampling of auxiliary fields can be achieved in several ways. The most intuitive one, in the spirit of Monte Carlo sampling, is to consider the Gaussian in the integral of Eq. (31) as a probability distribution. The sampled values are then used to determine the action of the operators on the spin part of the wave function. This is done exactly as in the diffusion process. It is possible to use other techniques to evaluate the integral (e.g., with the three-point Gaussian quadrature [27]), but results must be equivalent after the integration.

The method used to include the spin-orbit and three-nucleon interaction in the propagator and a detailed description of the AFDMC method can be found in Refs. [28–30].

C. Importance sampling

To reduce the variance of estimators, importance sampling is required. In practice, a diffusion Monte Carlo calculation is performed using a Green's function modified as follows:

$$\tilde{G}(\mathbf{R}, \mathbf{R}', \Delta\tau) = \frac{\psi_I(\mathbf{R}')}{\psi_I(\mathbf{R})} G(\mathbf{R}, \mathbf{R}', \Delta\tau). \tag{33}$$

The so-called importance function ψ_I in the above equation is often the same as that used for the projection of the energy and is evaluated at the walker configuration. More precisely, we define

$$\psi_I(\mathbf{R}) = \langle \psi_I | \mathbf{R} \rangle. \tag{34}$$

In this case, the distribution function that is sampled in the imaginary time converges to the quantity

$$f(\mathbf{R}, \tau \to \infty) = \psi_I(\mathbf{R}) \phi_0(\mathbf{R}). \tag{35}$$

The propagator becomes a shifted Gaussian with a modified weight

$$G_0(\mathbf{R},\mathbf{R}',\Delta\tau) = \left(\frac{1}{2\pi D\Delta\tau}\right)^{\frac{3A}{2}} \times \exp\left[-\frac{\left|\mathbf{R}-\mathbf{R}'+D\Delta\tau\frac{\nabla\psi_I(\mathbf{R})}{\psi_I(\mathbf{R})}\right|^2}{2D\Delta\tau}\right], \quad w = \exp\left[-\left(\frac{E_L(\mathbf{R})+E_L(\mathbf{R}')}{2}-E_T\right)\Delta\tau\right], \tag{36}$$

where $D=\hbar^2/m$ is the diffusion constant, and

$$E_L(\mathbf{R}) = -\frac{\hbar^2}{2m}\frac{\nabla^2\psi_I(\mathbf{R})}{\psi_I(\mathbf{R})} + \frac{V(\mathbf{R})\psi_I(\mathbf{R})}{\psi_I(\mathbf{R})} \tag{37}$$

is the local energy of the system. The additional term in the Gaussian is often called "drift", so each walker's configuration is diffused according to

$$\mathbf{R}' = \mathbf{R} + D\Delta\tau d + \boldsymbol{\eta}, \tag{38}$$

where the quantity

$$d = \frac{\nabla\psi_I(\mathbf{R})}{\psi_I(\mathbf{R})} \tag{39}$$

is the drift term, and η is a Gaussian random vector.

Importance sampling can also be included in the Hubbard-Stratonovich transformations that rotate nucleon spinors. For auxiliary fields, importance sampling is achieved by "guiding" the rotation given by each O_n operator. More precisely, one can consider the following identity:

$$-\frac{x_n^2}{2}+\sqrt{-\lambda_n\Delta\tau}x_nO_n = -\frac{x_n^2}{2}+\sqrt{-\lambda_n\Delta\tau}x_n\langle O_n\rangle+\sqrt{-\lambda_n\Delta\tau}x_n(O_n-\langle O_n\rangle),$$

where the mixed expectation value of the operator (see the next subsection for details) is evaluated in the old spin configuration:

$$\langle O_n\rangle = \frac{\langle\psi_I|O_n|R,S\rangle}{\langle\psi_I|R,S\rangle}. \tag{40}$$

This can be implemented by shifting the Gaussian used to sample auxiliary fields and considering the extra terms in the weight for branching, that is,

$$\exp\left[-x_n^2/2+\sqrt{-\lambda_n\Delta\tau}x_nO_n\right] = \exp[-(x_n-\bar{x}_n)^2/2]\exp[\sqrt{-\lambda_n\Delta\tau}x_nO_n] \times \exp\left[\bar{x}_nx_n-\bar{x}_n^2/2\right], \tag{41}$$

where

$$\bar{x} = \sqrt{-\lambda_n\Delta\tau}\langle O_n\rangle. \tag{42}$$

The additional weight term in Eq. (41) can also be included as a local potential, so it becomes

$$\exp\left[-\frac{\langle\psi_I|V|R,S\rangle}{\langle\psi_I|R,S\rangle}\Delta\tau\right]. \tag{43}$$

By combining the diffusion, the rotation, and all the additional factors, it is possible to write an explicit propagator

$$G(\mathbf{R},\mathbf{R}',\Delta\tau) = G_0(\mathbf{R},\mathbf{R}',\Delta\tau)\exp\left[-\left(-\frac{\hbar^2}{2m}\frac{\nabla^2|\psi_I(R,S)|}{|\psi_I(R,S)|} + \frac{\langle\psi_I|V|RS\rangle}{\langle\psi_I|RS\rangle}-E_0\right)\Delta t\right] \times \frac{\psi_I(R',S)}{\psi_I(R,S)}\frac{|\psi_I(R,S)|}{|\psi_I(R',S)|}, \tag{44}$$

where the drift term is

$$d = \frac{\nabla|\psi_I(R,S)|}{|\psi_I(R,S)|}. \tag{45}$$

D. Computation of expectation values

The projected walker distribution obtained with the AFDMC is used to compute expectation values. For a generic operator O in the limit $\tau\to\infty$, the "mixed" expectation value is computed as

$$\langle O\rangle_{\rm mix} = \frac{\langle\phi_0(\mathbf{R})|O|\psi_T(\mathbf{R})\rangle}{\langle\phi_0(\mathbf{R})|\psi_T(\mathbf{R})\rangle}. \tag{46}$$

We are interested in the expectation value over the ground state ϕ_0. Assuming that ψ_T is a good approximation of the ground state, a better estimate of the ground-state expectation value can be obtained by combining the variational Monte Carlo and the diffusion Monte Carlo estimators in this way:

$$\langle O\rangle = 2\langle O\rangle_{\rm mix} - \langle O\rangle_v, \tag{47}$$

where $\langle O\rangle_v$ is the expectation value computed over the variational wave function ψ_T used as trial wave function.

The evaluation of the energy of the system is a particular case and can be directly calculated from the projected distribution. Since the propagator commutes with the Hamiltonian (but this will change in the next section when we introduce a constraint), we have

$$\langle H\rangle_{\rm mix} = \frac{\langle\phi_0(\mathbf{R})|H|\psi_T(\mathbf{R})\rangle}{\langle\phi_0(\mathbf{R})|\psi_T(\mathbf{R})\rangle} = \frac{\langle\psi_T(\mathbf{R})|H|\phi_0(\mathbf{R})\rangle}{\langle\psi_T(\mathbf{R})|\phi_0(\mathbf{R})\rangle} = E_0. \tag{48}$$

The total energy is already the correct value, and since it does not contain a linear error from the trial function, it does not require the extrapolation of Eq. (47).

The propagator used in our AFDMC calculations is written to include only the first eight operators of the Argonne interactions. However, in some cases, we can also evaluate the expectation value of the full Argonne v_{18} Hamiltonian. In light nuclei, the expectation value of Argonne v_8' is within few percent of Argonne v_{18} [7]. It is then reasonable to propagate the wave function using the Argonne v_8' and evaluate the difference between Argonne v_8' and v_{18} using the extrapolation of Eq. (47). This procedure was verified in GFMC calculations [13], and we employed this technique in the case of low density where Argonne v_8' is a very good approximation to Argonne v_{18}.

More precisely, we evaluate the energy using Argonne v_8' in the propagator (in addition to the three-nucleon interaction),

and we add to the total energy the value of $\langle v_{18} - v_8' \rangle$ evaluated as in Eq. (47). We expect this approximation to be accurate if this difference is small as in light nuclei.

E. Constrained path and fixed-phase approximation

As described in the above sections, the diffusion Monte Carlo method projects out the ground state of a given Hamiltonian in terms of the distribution of the walkers. However, the density of walkers must always be positive definite [31]. For walkers with positive weights, this condition restricts, in principle, the use of the method to that class of problems where the trial wave function is always positive or is node-less, such as for a Bose system in the ground state. Algorithms that allow negative weights, such as transient estimation [32], generally have exponentially increasing variance.

One way to deal with fermionic systems is to set artificial boundary conditions between the positive and negative regions of the trial wave function. It is possible to define a nodal surface where the trial wave function is zero and during the diffusion process, a walker that crosses the nodal surface is dropped; this is the fixed-node approximation [32,33], and its application in the diffusion Monte Carlo algorithm always gives an upper bound to the true fermionic ground-state energy.

In the case of nuclear Hamiltonians or for problems where the trial wave function must be complex, a constrained-path [34–36] approximation is usually applied to avoid the fermion sign or phase problem. The constrained-path method was originally proposed by Zhang *et al.* as a generalization of the fixed-node approximation to complex wave functions. In constrained-path, walkers are constrained to regions where the real part of the overlap with the trial wave function is positive. This constrained-path approximation was the original method used to control the phase problem in the AFDMC algorithm [10]. More precisely, we have to consider that even for a complex wave function, the drift term for the coordinates must be real. In the constrained-path approximation, a natural choice for the drift is

$$d = \frac{\nabla \mathrm{Re}[\psi_I(\mathbf{R})]}{\mathrm{Re}[\psi_I(\mathbf{R})]}. \tag{49}$$

Moreover, to eliminate the decay of the signal-to-noise ratio, it is possible to impose the constrained-path approximation by requiring that the real part of the overlap of each walker with the trial wave function keeps the same sign. Thus, one can impose

$$\frac{\mathrm{Re}[\psi_I(\mathbf{R}')]}{\mathrm{Re}[\psi_I(\mathbf{R})]} > 0, \tag{50}$$

where $\mathbf{R}$ and $\mathbf{R}'$ denote the coordinates of the system after and before the diffusion of a time step. If this condition is violated, the walker is dropped. This form was found to give better results and was employed in previous AFDMC calculations [37,38].

An alternative way to control the sign problem is the fixed-phase approximation. This method was originally proposed by Carlson for nuclear systems [39] and also employed for systems whose Hamiltonians contain a magnetic field [40].

We start with the same condition of the reality of the drift, and we consider the following expression

$$d = \frac{\nabla |\psi_I(\mathbf{R})|}{|\psi_I(\mathbf{R})|}. \tag{51}$$

With this choice the weight for branching becomes

$$\exp\left[-\left(-\frac{\hbar^2}{2m}\frac{\nabla^2|\psi_I(\mathbf{R})|}{|\psi_I(\mathbf{R})|} + \frac{V\psi_I(\mathbf{R})}{\psi_I(\mathbf{R})}\right)\Delta\tau\right] \times \frac{|\psi_I(\mathbf{R})|}{|\psi_I(\mathbf{R}')|}\frac{\psi_I(\mathbf{R}')}{\psi_I(\mathbf{R})}. \tag{52}$$

Note that in this expression there is the usual importance sampling factor as in Eq. (33) and an additional factor that corrects for the particular choice of the drift.

A generic complex wave function can be written as

$$\psi(\mathbf{R}) = |\psi(\mathbf{R})| e^{i\phi(\mathbf{R})}, \tag{53}$$

where $\phi(\mathbf{R})$ is the phase of $\psi(\mathbf{R})$; the factor appearing in Eq. (52) can be rewritten as

$$\frac{|\psi_I(\mathbf{R})|}{|\psi_I(\mathbf{R}')|}\frac{\psi_I(\mathbf{R}')}{\psi_I(\mathbf{R})} = e^{i[\phi(\mathbf{R}')-\phi(\mathbf{R})]}. \tag{54}$$

The fixed-phase approximation constrains the walkers to have the same phase as the importance function ψ_I. It can be applied by keeping the real part of the last expression. To keep fixed the normalization of the Green's function, one has an additional factor in the Green's function that must be included in the weight:

$$\exp\left[-\frac{\hbar^2}{2m}(\nabla\phi)^2\,\Delta\tau\right]. \tag{55}$$

This can be automatically included by keeping the real part of the kinetic energy. In fact,

$$\mathrm{Re}\left[\frac{\nabla^2\psi_I(\mathbf{R})}{\psi_I(\mathbf{R})}\right] = \frac{\nabla^2|\psi_I(\mathbf{R})|}{|\psi_I(\mathbf{R})|} - (\nabla\phi(\mathbf{R}))^2. \tag{56}$$

The real part of the kinetic energy includes the additional weight term given by the fixed-phase approximation.

A different derivation for introducing the fixed-phase approximation is the following. Let us consider the evolution of a complex trial wave function including the importance sampling:

$$\psi_I^*(\mathbf{R})\psi(\mathbf{R},\tau) = \int G(\mathbf{R},\mathbf{R}',\tau)\psi_I^*(\mathbf{R})\psi(\mathbf{R}',0)\,d\mathbf{R}'. \tag{57}$$

The quantity $\psi_I^\star(\mathbf{R})\psi(\mathbf{R},\tau)$ is not real and positive definite as required, but it is possible to obtain another positive density as

$$|\psi_I(\mathbf{R})||\psi(\mathbf{R},\tau)| = \int G(\mathbf{R},\mathbf{R}',\tau)\frac{|\psi_I(\mathbf{R})|}{|\psi_I(\mathbf{R}')|}e^{i[\phi(\mathbf{R}')-\phi(\mathbf{R})]} \times |\psi_I(\mathbf{R}')||\psi(\mathbf{R}',0)|d\mathbf{R}'. \tag{58}$$

In this way, we impose that the phase of the trial wave function is the same of that of ψ_I.

Both the constrained-path and the fixed-phase approximations deal with the fermion sign problem, and in principle they should be equivalent if the importance function is close to the correct ground state of the system.

It is important to note that Carlson *et al.* [41] showed that within the constrained-path approximation, the algorithm does not necessarily give an upper bound in the calculation of energy. This was also observed by Wiringa *et al.* in some nuclear simulations using the GFMC technique [42]. It is not guaranteed that our fixed-phase calculations give an upper bound. However, in diffusion Monte Carlo calculations of the ground state of quantum dots, where either a real or a complex trial wave function can be implemented, the fixed-phase approximation gives a higher energy than the fixed-node approximation [43].

F. Trial wave function

The trial wave function used as the importance and projection function for the AFDMC algorithm has the following form:

$$\psi_I(\mathbf{R}, S) = F_J(\mathbf{R}) D(\mathbf{R}, S), \tag{59}$$

where $\mathbf{R} \equiv (\mathbf{r}_1, \ldots, \mathbf{r}_N)$ represent the spatial and $S \equiv (s_1, \ldots, s_N)$ are the spin states of the system. The spin assignments s_i consist of giving the two-spinor components for each neutron, namely,

$$|s_i\rangle = a_i|\uparrow\rangle + b_i|\downarrow\rangle, \tag{60}$$

where a_i and b_i are complex numbers, and $\{|\uparrow\rangle, |\downarrow\rangle\}$ is the neutron-up and neutron-down basis.

The Jastrow correlation function $F_J(\mathbf{R})$ is symmetric under the exchange of two particles and independent of spin. Its role is to include the short-range pair correlations in the trial wave function. The generic form for the Jastrow is

$$F_J(\mathbf{R}) = \prod_{i<j} f(r_{ij}), \tag{61}$$

where the function $f(r)$ is the solution of a Schrödinger-like equation for $f(r < d)$,

$$-\frac{\hbar^2}{m}\nabla^2 f(r) + v(r) f(r) = \lambda f(r), \tag{62}$$

where $v(r)$ is the spin-independent part of the nucleon-nucleon interaction, the healing distance $d < L/2$ is a variational parameter, and L is the size of the box. For distances $r \geqslant d$, we impose $f(r) = 1$. The Jastrow part of the trial wave function in the AFDMC case has only the role of reducing the overlap of neutrons, therefore reducing the energy variance. Since it does not change the phase of the wave function, it does not influence the computed energy value in projections methods. In all the reported results, we then fixed $d = 2$ fm or $d = L/2$ if $L/2 < 2$ fm.

The antisymmetric part of the trial wave function is usually given by the ground state of the noninteracting fermions, which is written as a Slater determinant

$$D(\mathbf{R}, S) = \mathcal{A}\left[\prod_{i=1}^{N} \phi_\alpha(\mathbf{r}_i, s_i)\right] = \mathrm{Det}\left\{\phi_\alpha(\mathbf{r}_i, s_i)\right\}, \tag{63}$$

where α is the set of quantum numbers of single-particle orbitals, and $\mathcal{A}$ is the antisymmetrization operator.

For neutron matter calculations, we choose the antisymmetric part as the ground state of the Fermi gas, built from a set of plane waves. The infinite uniform system is simulated with N nucleons in a cubic periodic box of volume L^3. The momentum vectors in this box are

$$\mathbf{k}_\alpha = \frac{2\pi}{L}(n_{\alpha x}, n_{\alpha y}, n_{\alpha z}), \tag{64}$$

where α labels the quantum state and n_x, n_y and n_z are integer numbers describing the state. The single-particle orbitals are given by

$$\phi_\alpha(\mathbf{r}_i, s_i) = e^{i\mathbf{k}_\alpha \cdot \mathbf{r}_i}\langle \chi_{s,m_s,\alpha}|s_i\rangle. \tag{65}$$

G. Twist-averaged boundary conditions

Aside from the effect of the phase of the importance function employed during the projection in imaginary time, the dependence of the energy on the number of neutrons is the largest systematic error. Usually one uses periodic boundary conditions to reduce finite-size effects, and simulations are carried out by using a number of neutrons filling closed shells of plane waves. There are still sizable errors in the kinetic energy coming from the shell structure even at the closed shell filling in momentum space (1, 7, 19, 27, 33, 57, . . .). To establish the effect of the finite size of the system due to the kinetic energy, we imposed twist-averaged boundary conditions [44] on the trial wave function. Within periodic boundary conditions, the phase, which is picked up by the wave function as a particle makes a circuit across the unit cell, can be chosen arbitrarily. These more general boundary conditions for a wave function are

$$\psi(\mathbf{r}_1 + L\hat{\mathbf{x}}, \mathbf{r}_2, \ldots) = e^{i\theta_x}\psi(\mathbf{r}_1, \mathbf{r}_2, \ldots), \tag{66}$$

where L is the side of the simulation cell. The boundary condition $\theta = 0$ gives the usual periodic boundary conditions, and the more general condition with $\theta \neq 0$ gives the twisted boundary conditions. If the twist angle is integrated over, the single-particle finite-size effects, arising from shell effects in filling the plane wave orbitals, are substantially reduced. Integrating over twists averages over the volume of $\mathbf{k}$ space occupied by the first N Brillouin zones of the simulation cell. The occupied region is a convex polyhedron that tends to the Fermi surface in the limit of an infinite system size and has the correct volume at all system sizes. The twist-averaged kinetic energy must approach the exact energy always from above, since the single-particle kinetic energy is a convex function of $\mathbf{k}$.

The integration over angles can be achieved in different ways, either by modifying the trial wave function during the simulation or by performing several simulations using different wave functions [44]. In practice, once the density of the system is fixed, we consider a grid of different $\mathbf{k}_i$ vectors

$$\mathbf{k}_{\alpha,i} = (2\pi\mathbf{n}_\alpha + \theta_i)/L \tag{67}$$

within the radius corresponding to the Fermi energy; and for each twist angle θ_i, a simulation is performed. The total energy is given by averaging all the energies obtained for each wave function.

H. Algorithm

The structure of the AFDMC algorithm consists of the following procedures:

(i) Sample the positions and spins, to give $|R, S\rangle$ for the initial walkers, from $|\langle\Psi_I|R, S\rangle|^2$ using the Metropolis Monte Carlo method.
(ii) Propagate the spatial degrees of freedom as in the usual diffusion Monte Carlo with a drifted Gaussian for a time step. That is, each walker configuration is diffused according to Eq. (38).
(iii) For each walker, build and diagonalize the potential matrix $A^{(\sigma)}$.
(iv) Loop over the eigenvectors, sampling the corresponding shifted Hubbard-Stratonovich variable, and update the spinors for a time step. Introduce approximate importance sampling of the Hubbard-Stratonovich variables, as discussed in the previous sections.
(v) Propagate with the spin–orbit interaction, using importance sampling.
(vi) Evaluate the real part of the local energy to constrain each walker to have a fixed phase as described above. This quantity is also stored with the corresponding weight to calculate the averaged mixed energy.
(vii) Iterate from 2 to 6 as long as necessary until convergence of the energy is reached.

To evaluate the error bars, block averages are calculated and the results combined over different block sizes until the blocks become uncorrelated and the error bars independent of block size within statistics.

IV. RESULTS

A. Test of the fixed-phase approximation

The AFDMC algorithm combined with the constrained-path approximation was previously employed by Sarsa *et al.* to study the neutron matter equation of state at zero temperature [28]. In that paper, the Hamiltonian contained both a realistic Argonne v_8' two-nucleon and the Urbana-IX three-nucleon interactions; this Hamiltonian is often used to calculate properties of both symmetric nuclear matter and pure neutron matter.

The constrained-path AFDMC proved to give very satisfactory results for neutron matter calculations with two- and three-nucleon interactions, but some problems were encountered in the evaluation of the spin-orbit contribution. The inclusion of spin-backflow correlations reduced the discrepancies. A detailed study considering a pure nucleon-nucleon interaction emphasized the problem of constrained-path AFDMC in dealing with the spin-orbit interaction [45]. A similar behavior was found by comparing the constrained-path AFDMC with the GFMC evaluation for the energy of 14 neutrons in a periodic box [9]. When using the same Hamiltonian with the same box truncation used in GFMC calculations of Ref. [9], the constrained-path AFDMC overestimated the energy of 14 neutrons with an Argonne v_8' interaction.

The AFDMC with the fixed-phase approximation overcomes the discrepancies previously observed in the estimates of the spin-orbit contribution to the total energy, as shown in Table I. Without tail corrections, the constrained-path AFDMC energy of 14 neutrons at $\rho = 0.16$ fm^{-3} is 20.32(6) MeV compared to 17.00(27) MeV given by the unconstrained GFMC [9], while the fixed-phase AFDMC energy is 17.67(5) MeV, within 3%, and in much better agreement with unconstrained GFMC.

TABLE I. Fixed-phase (FP-AFDMC) energies per particle of 14 neutrons interacting with the Argonne v_8' interaction in a periodic box without the inclusion of finite-size effects at various densities. The constrained-path (CP-AFDMC) of Ref. [28], the constrained-path (CP-GFMC) and the unconstrained (UC-GFMC) GFMC of Ref. [9] are also reported for a comparison. All energies are expressed in MeV.

ρ (fm^{-3})	FP-AFDMC	CP-AFDMC	CP-GFMC	UC-GFMC
0.04	6.75(7)		6.43(01)	6.32(03)
0.08	10.29(1)		10.02(02)	9.591(06)
0.16	17.67(5)	20.32(6)	18.54(04)	17.00(27)
0.24	27.7(5)		30.04(04)	28.35(50)

For the higher densities reported in Table I, it should be noted that the constrained-path GFMC significantly differs from unconstrained GFMC because the fermion sign problem becomes more severe and the unconstrained energy estimation has larger fluctuations. The convergence can be hard to reach because the imaginary time evolution of the energy can be carried out only for very small steps. These reasons could introduce some spurious effects limiting the accuracy of GFMC for the neutron matter calculation to densities below 0.08 fm^{-3} [9].

Preliminary results for the ground-state calculation of neutron drops by means of the fixed-phase AFDMC show that the spin-orbit contribution is now in agreement with the GFMC results [30]. Using the same Hamiltonian, previous constrained-path AFDMC calculations predicted a spin-orbit splitting (SOS) in the $7n$ neutron drop of about half the GFMC result [29]. Instead, the fixed-phase AFDMC estimate is in excellent agreement with the GFMC one [30], also for neutron drops containing up to 13 neutrons [46].

The improvement obtained by using the fixed-phase approximation rather than the constrained-path is also evident in the comparison of the fixed-phase AFDMC with the available constrained-path AFDMC using spin-backflow correlations. In Table II, we report all the available calculations computed within the constrained-path approximation compared to the fixed-phase one. The corrections included are only due to the truncation of the nucleon-nucleon interaction as in the old calculations [28].

B. Equation of state of neutron matter

We employed the fixed-phase AFDMC method to study neutron matter by simulating different numbers of neutrons interacting with the Argonne v_8' potential, including finite-size corrections as described in Ref. [28]. All the fixed-phase AFDMC results are reported in Table III, which shows the energy per neutron of neutron matter for different densities by varying the number of neutrons.

TABLE II. Fixed-phase (FP-AFDMC) energies per particle of 14 and 66 neutrons interacting with the Argonne v_8'+Urbana-IX interaction in a periodic box at various densities compared with the available constrained-path (CP-AFDMC) ones of Ref. [28]. The constrained-path AFDMC results using a Jastrow-Slater-backflow (JSB) wave function [47] are also shown. To make the comparison possible, the finite-size effect due to the truncation of nucleon-nucleon interaction was included, while that of Urbana-IX was omitted. All energies are expressed in MeV.

ρ (fm^{-3})	FP-AFDMC(14)	CP-AFDMC(14)	JSB-AFDMC(14)
0.12	14.52(5)	14.80(9)	
0.16	19.03(7)	19.76(6)	
0.20	24.49(5)	25.23(8)	
0.32	46.60(8)	48.4(1)	46.8(1)
ρ (fm^{-3})	FP-AFDMC(66)	CP-AFDMC(66)	JSB-AFDMC(66)
0.12	15.04(8)	15.26(5)	
0.16	20.14(5)	20.23(9)	
0.20	26.21(5)	27.1(1)	
0.32	52.47(4)	54.4(6)	52.9(2)

Some finite-size effects are present, as can be deduced by observing the energies for different numbers of neutrons. The same behavior is followed at each density, and $E(38) < E(14) < E(66)$. This trend directly follows the kinetic energy oscillations of N free fermions, which for $N = 38$ is lower than either $N = 14$ or $N = 66$.

For neutron matter, the Urbana-IX three-nucleon force reduces to a pairwise spin interaction modulated by the spectator neutron as explained in Refs. [29,30] which can be easily included into the propagator. Finite-size corrections due to the Urbana-IX can be included in the same way as for the nucleon-nucleon interaction, although their contribution is very small compared to the potential energy. Their effect is appreciable only for a small number of particles and at large density, i.e., if the size of the simulation box is small.

TABLE III. Fixed-phase AFDMC energies per particle of 14, 38, and 66 neutrons interacting by the Argonne v_8' potential in a periodic box at various densities. The finite-size effects due to the nucleon-nucleon truncation are included. All energies are expressed in MeV.

ρ (fm^{-3})	E/N (14)	E/N (38)	E/N (66)
0.12	12.08(5)	11.18(4)	12.65(4)
0.16	14.87(9)	13.50(5)	15.43(3)
0.20	17.6(1)	16.10(4)	18.27(5)
0.24			21.56(5)
0.28			25.05(6)
0.32	27.2(1)	25.2(1)	28.93(7)
0.36			33.05(6)
0.40			37.15(8)
0.48			46.7(1)
0.56			57.64(9)
0.64			69.90(8)
0.80	91.5(2)	89.2(2)	97.4(1)

TABLE IV. Fixed-phase AFDMC energies per particle of 14, 38, 66, and 114 neutrons interacting by the Argonne v_8'+Urbana-IX potential in a periodic box at various densities. Note the difference from the values of Table II due to the different treatment of finite-size effects, which, in this case, include two- and three-nucleon interaction contributions. All energies are expressed in MeV.

ρ (fm^{-3})	E/N(14)	E/N(38)	E/N (66)	E/N (114)
0.12	14.77(7)	13.68(3)	15.18(2)	16.05(4)
0.16	19.41(7)	18.32(4)	20.04(2)	21.31(4)
0.20	25.05(7)	24.06(4)	26.13(4)	27.82(5)
0.24	31.74(6)		33.64(4)	
0.28	39.79(3)		42.51(3)	
0.32	48.61(5)	48.76(6)	51.84(2)	55.13(6)
0.36	60.03(5)		64.89(5)	
0.40	72.38(5)		78.59(6)	
0.48	102.74(5)		111.69(9)	
0.56	139.8(1)		152.81(2)	
0.64			202.19(9)	
0.80		320.3(1)	328.19(6)	

All the fixed-phase AFDMC results of 14, 38, 66, and 114 neutrons interacting with the Argonne v_8' Urbana-IX Hamiltonian, including all the finite-size effects due to the truncation of two- and three-nucleon interactions, are summarized in Table IV. Important finite-size effects are still present. The value closest to the thermodynamic limit is that for 66 neutrons, because the free Fermi gas energy of this particular system is very similar to that of the infinite one. However, the difference of the energy of 66 and 114 neutrons is always within 6–7%. This behavior was also observed in a study of finite-size effects using the periodic box FHNC technique [48], and the analysis of Sarsa *et al.* [28] suggests that the energy of the system in the infinite limit is somewhere between the energies of 66 and 114 neutrons.

To better understand the finite-size effects due to the kinetic energy, we repeated several simulations by imposing twist-averaged boundary conditions in the trial wave function. The results are displayed in Fig. 1, where we reported the energy obtained by averaging all the results using sets of ten twist angles in each dimension. The different behavior of the energy as a function of the number of neutrons using periodic or twist-averaged boundary conditions is well evident. As expected the effect of twist averaging is to reduce the jumps of the energy as a function of N given by periodic boundary conditions. Then the extrapolation to the infinite limit of N is better evident using twist averaging. However it is remarkable that the energy of 66 neutrons computed using either twist averaging or periodic boundary conditions is almost the same. This essentially follows the fact that the kinetic energy of 66 fermions approaches the infinite limit very well. In addition, the twist averaging could be very useful in simulating systems for which an arbitrary number of fermions is needed [49].

In Fig. 2, we plot the fixed-phase AFDMC equation of state, obtained with the energy of 66 neutrons, and the calculation of Akmal *et al.* [50], where the Argonne v_{18} interaction combined with the Urbana-IX three-nucleon interaction was considered.

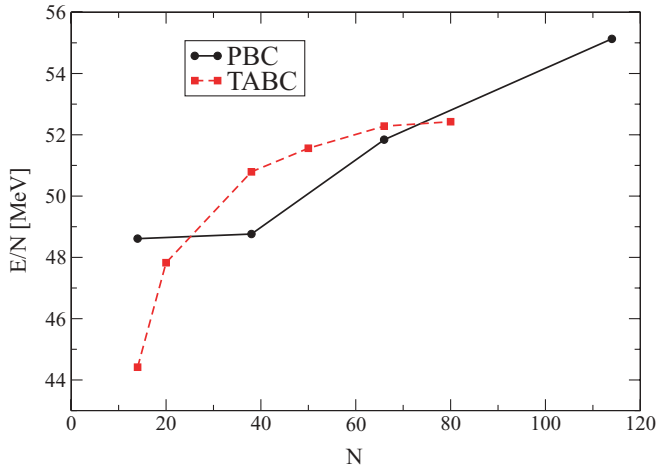

FIG. 1. (Color online) Convergence of the computed energy at $\rho = 0.32$ fm^{-3} as a function of neutrons in a box within the grid twist-averaging method (TABC) described in the text with ten twists: the Argonne v_8'+Urbana-IX Hamiltonian were considered. The equation of state is compared with the fixed-phase AFDMC calculations with periodic boundary conditions (PBC) shown by solid lines.

As can be seen, both the Argonne v_8' and v_{18} give an equation of state showing essentially the same behavior, with a difference in the energy that is similar throughout the considered range of densities. The addition of the three-nucleon interaction increases the differences between the AFDMC and the Akmal *et al.*, in particular at higher densities, implying a strong difference in pressure and compressibility.

The Argonne v_8' interaction should be more attractive than Argonne v_{18} as shown in light nuclei and in neutron-drop calculations [13]. The plots shown in Fig. 2, however, where we compare Argonne v_8' results with the v_{18} values of Akmal *et al.*, do not show this. We believe this is indicative of systematic errors in the FHNC/SOC calculations. The fixed-phase AFDMC has proved to be in very good agreement with the GFMC results for light nuclei [11] and also with the GFMC results for 14 neutrons. On the other hand, the fixed-phase AFDMC calculation of nuclear matter suggests that the FHNC/SOC approximation could miss important contributions, in particular those coming from the neglected elementary diagrams in the FHNC summation [12]. In the Akmal *et al.* calculations, the energy is computed by means of a cluster expansion for which no evidence of convergence can be provided. The addition of the Urbana-IX three-body interaction to the Hamiltonian increases the differences between the AFDMC results and those of Akmal *et al.*, and, again, this confirms that the variational technique based on the cluster expansion gives a lower energy because it neglects important contributions. However, we stress the fact that in the case of neutron matter, the contribution of the tensor-τ force is small compared to the other channels of the interaction. For this reason, the calculation of the energy within traditional variational techniques based on FHNC/SOC or cluster expansion could be more accurate for pure neutron matter without protons. This is not true when dealing with nuclear matter in which the effect of tensor-τ is most important, as confirmed in Ref. [12].

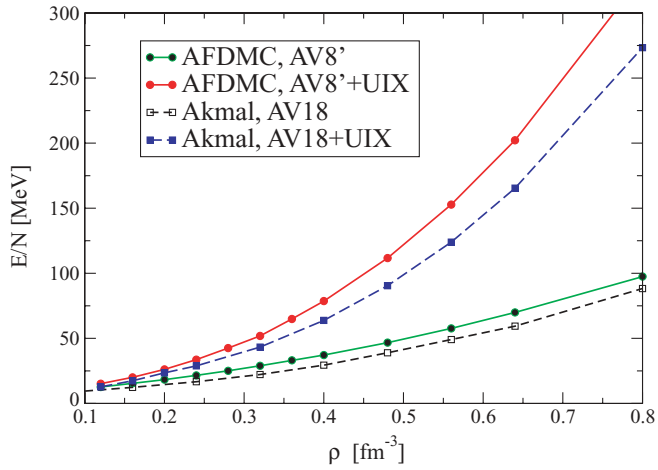

FIG. 2. (Color online) Fixed-phase AFDMC equation of state evaluated by simulating 66 neutrons in a periodic box; the Argonne v_8' (AV8′) and Argonne v_8'+Urbana-IX (AV8′+UIX) Hamiltonians were considered. The equation of states are compared with the variational calculations of Ref. [50] using the Argonne v_{18} (AV18) and the Argonne v_{18}+Urbana-IX (AV18-UIX) Hamiltonians. See the legend for details.

The AFDMC results have been fitted with the following functional form:

$$\frac{E}{N}(\rho) = a\rho^{\beta} + c\rho^{\gamma}, \tag{68}$$

where E/N is the energy per neutron in MeV as a function of density in fm^{-3}. The parameters of the fit for both Argonne v_8' and the full Argonne v_8'+Urbana-IX Hamiltonian are reported in Table V. We also tried to use the functional form of Ref. [51], where $\beta = 1$. We had a worse χ^2, but the equation of state and the pressure as a function of the density does not change in a significant way.

C. Argonne v_8' and v_{18} interactions

As described in the above sections, in most cases the Argonne v_{18} result is evaluated as a perturbation of the Argonne v_8' [13]. The assumption is reasonable, since the Argonne v_8' potential contains most of the contributions of v_{18} potential and was obtained with a reprojection by keeping only the most important terms. However, the operators appearing in Argonne v_{18} and not in Argonne v_8' are not exactly included in the GFMC calculations. The imaginary-time GFMC evolution is performed using Argonne v_8', and the energy is calculated perturbatively in the difference between v_8' and v_{18}, which for nuclei is a fraction of an MeV.

TABLE V. Parameters of Eq. (68) fitting the equation of state computed with the full Argonne v_8'+Urbana-IX (AV8′+UIX) Hamiltonian and with the nucleon-nucleon interaction only (AV8′). The parameters a and c are expressed in MeV/fm^{-3}.

Hamiltonian	a	c	β	γ
AV8′	23.0	115.7	0.37	1.87
AV8′+UIX	32.6	507.8	0.48	2.375

This method is also used in the FHNC/SOC calculation, where only the lowest order two-body nucleon-nucleon correlations are included in the variational wave function [50]. However, there is no reason to believe that such a calculation gives an upper bound to the true energy, and this approximation may not be good, particularly for higher densities.

When using a propagator including the Argonne v_8' potential, the difference between the energies computed using Argonne v_8' and v_{18} is actually very small. For instance, for 14 neutrons at $\rho \leqslant 0.12$ fm^{-3}, the difference between Argonne v_8' and v_{18} is less than 2 MeV per neutron and is 2.7 and 5.1 MeV for densities of 0.16 and 0.20 fm^{-3}, respectively. On the other hand, a plain truncation of Argonne v_{18} in the propagator leads to huge energy differences in the two estimates. At $\rho = 0.12$ fm^{-3}, the energy of 14 neutrons with the Argonne v_8'+Urbana-IX Hamiltonian is 14.12 MeV, while it is 3.60 MeV for Argonne v_{18}+Urbana-IX. This means that the extra v_{18} terms cannot be thought of as a small correction to Argonne v_8', at least in this range of densities. However, at $\rho \leqslant 0.04$ fm^{-3}, the difference between Argonne v_8' and v_{18} is a few percent of the total energy, so we can safely evaluate this difference as a perturbation using the v_8' propagator.

In the very low-density regime, neutron matter is a superfluid gas, and a trial wave function written in a BCS form including explicitly the pairing between neutrons is needed [52,53]. However, we expect that the expectation value of the Argonne v_8' interaction to be of the order of that of Argonne v_{18} both in the superfluid and in the normal phase. Here we are only interested in a qualitative study of the difference between Argonne v_8' and v_{18}, thus a wave function as presented in Sec. III F was used, rather then that of Ref. [38].

It is interesting to focus on the equation of state of neutron matter in the low-density regime and in the normal phase. The Argonne v_{18}+Urbana-IX Hamiltonian as described was used. The range of $\rho \leqslant 0.04$ fm^{-3} is particularly relevant in the study of properties of the inner crust of neutron stars. The very low-density neutron matter approaches a regime that is almost universal and is analogous to, for instance, cold atoms [54]. In this regime, many-body techniques can be compared and calibrated [55,56].

We report the energy of 66 neutrons in a periodic box in Table VI. The Hamiltonian uses the Argonne v_8'+Urbana-IX potential, and the potential is corrected for finite-size effects.

TABLE VI. Fixed-phase AFDMC energies per particle of 66 neutrons interacting with the Argonne v_8'+Urbana-IX interaction in a periodic box at various densities. The difference between the v_8' and the v_{18} interactions (AV8′−AV18), evaluated with an extrapolation as described in Sec. III D is also reported. All energies are expressed in MeV.

ρ (fm^{-3})	E/N	⟨AV8′−AV18⟩
3.377×10^{-5}	0.089(1)	−0.00197574
2.702×10^{-4}	0.367(2)	0.0002776
0.002162	1.289(2)	0.002525
0.007295	2.606(4)	0.021712
0.01729	4.277(7)	0.082534
0.03377	6.197(2)	0.30802

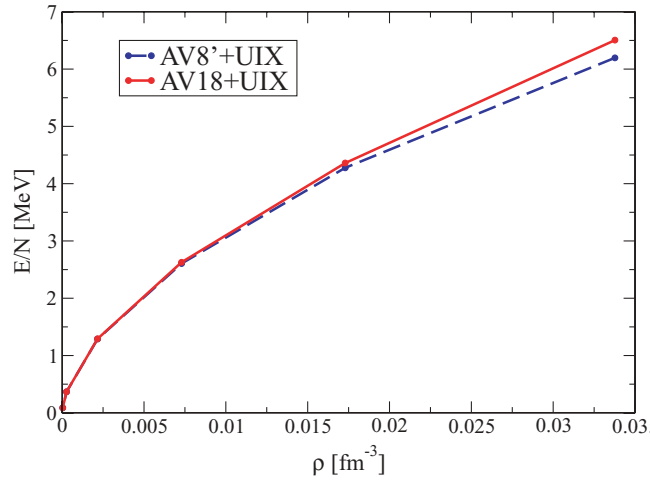

FIG. 3. (Color online) Equation of state of neutron matter in the low-density regime. The Argonne v_8' (AV8′) and v_{18} (AV18) interactions combined with the Urbana-IX (UIX) three-nucleon interaction were considered as indicated in the legend.

The difference between the Argonne v_8' and the v_{18} interactions was extrapolated as described in Sec. III D. As can be seen, at such densities the Argonne v_{18} contribution is similar to v_8', of the order of a few percent with respect to the total energy. We believe that such a difference would be even smaller if the full Argonne v_{18} was implemented in the propagator and then evaluated without the extrapolation described in the above sections.

The equation of state of neutron matter in the low-density regime is reported in Fig. 3, where the energy per neutron as a function of the density is calculated both with the AV8′ and with the AV18 nucleon-nucleon interaction combined with the Urbana-IX three-nucleon interaction. It can be seen that the difference between the two Hamiltonians considered is very small in this regime. The Argonne v_8' and v_{18} combined with the Urbana-IX essentially give the same energy, and only small deviations are present when the density increases above $\approx$0.015 fm^{-3}. This result is confirmed by the fact that in such a regime the neutron-neutron interaction is dominated by the S channel, which in the Argonne v_8' is the same as in v_{18} [57]. There is a small trend that the energies are sensibly higher at $\rho \leqslant 0.015$ fm^{-3}. Other many-body calculations are in general not in agreement and present very different behaviors in this regime [58].

V. CONCLUSIONS

We accurately calculated the equation of state of neutron matter using the auxiliary field diffusion Monte Carlo method. We started from a nonrelativistic nuclear Hamiltonian containing two- and three-nucleon potentials. The AFDMC algorithm suffers from the usual fermion sign problem present in all fermionic Monte Carlo calculations, and we find that the fixed-phase approximation used to control it to be more accurate than the previously used constrained-path approximation. In particular, in this work we demonstrated that the fixed-phase AFDMC overcomes the problems encountered when dealing

with the spin-orbit interaction. The Urbana-IX three-body force is included in the fixed-phase AFDMC calculation without any perturbative evaluation, because it is naturally included in the Green's function used for the propagation. The fixed-phase AFDMC reveals some problems of the variational cluster summation (or FHNC/SOC) technique just highlighted in the nuclear matter calculation with a simple v_6-like interaction [12].

We computed the equation of state of neutron matter using a modern, but still simplified, nucleon-nucleon interaction combined with a realistic three-nucleon interaction in the regime of interest for predicting the properties of neutron stars, and we found some deviations with respect to past variational calculations based on cluster expansion, in particular at high densities. The difference between the Argonne v_8'+Urbana-IX Hamiltonian and that containing the more sophisticated Argonne v_{18} interaction was perturbatively evaluated in the low-density regime, where the equation of state is useful in constraining properties of the inner crust of neutron stars. Our equation of state can also be useful in comparing the wide range of Skyrme forces used to study the neutron matter.

We are working to include the full Argonne v_{18} interaction in the two-body part of the Hamiltonian, and we are investigating the effect of the more complex Illinois three-nucleon forces. The effect of those forces in neutron drops and in neutron matter will be a subject of future work.

ACKNOWLEDGMENTS

We thank J. Carlson, S. C. Pieper, and R. B. Wiringa for useful discussions. This work was supported in part by NSF grants PHY-0456609 and PHY-0757703. Calculations were performed partially on the HPC facility "BEN" at ECT* in Trento under a grant of Supercomputing Projects, partially on the HPC facility of SISSA/Democritos in Trieste, and partially on the HPC facility "WIGLAF" of the Department of Physics, University of Trento.

[1] G. G. Raffelt, *Stars as Laboratories for Fundamental Physics: The Astrophysics of Neutrinos, Axions, and Other Weakly Interacting Particles* (University of Chicago, Chicago, 1996).
[2] P. Danielewicz, R. Lacey, and W. G. Lynch, Science **298**, 1592 (2002).
[3] B. A. Brown, Phys. Rev. Lett. **85**, 5296 (2000).
[4] J. R. Stone, J. C. Miller, R. Koncewicz, P. D. Stevenson, and M. R. Strayer, Phys. Rev. C **68**, 034324 (2003).
[5] V. R. Pandharipande and R. B. Wiringa, Rev. Mod. Phys. **51**, 821 (1979).
[6] J. Morales, V. R. Pandharipande, and D. G. Ravenhall, Phys. Rev. C **66**, 054308 (2002).
[7] S. C. Pieper, V. R. Pandharipande, R. B. Wiringa, and J. Carlson, Phys. Rev. C **64**, 014001 (2001).
[8] S. C. Pieper, Nucl. Phys. **A751**, 516 (2005).
[9] J. Carlson, J. Morales, V. R. Pandharipande, and D. G. Ravenhall, Phys. Rev. C **68**, 025802 (2003).
[10] K. E. Schmidt and S. Fantoni, Phys. Lett. **B446**, 99 (1999).
[11] S. Gandolfi, F. Pederiva, S. Fantoni, and K. E. Schmidt, Phys. Rev. Lett. **99**, 022507 (2007).
[12] S. Gandolfi, F. Pederiva, S. Fantoni, and K. E. Schmidt, Phys. Rev. Lett. **98**, 102503 (2007).
[13] B. S. Pudliner, V. R. Pandharipande, J. Carlson, S. C. Pieper, and R. B. Wiringa, Phys. Rev. C **56**, 1720 (1997).
[14] V. G. J. Stoks, R. A. M. Klomp, M. C. M. Rentmeester, and J. J. de Swart, Phys. Rev. C **48**, 792 (1993).
[15] V. G. J. Stoks, R. A. M. Klomp, C. P. F. Terheggen, and J. J. de Swart, Phys. Rev. C **49**, 2950 (1994).
[16] R. B. Wiringa, V. G. J. Stoks, and R. Schiavilla, Phys. Rev. C **51**, 38 (1995).
[17] R. B. Wiringa and S. C. Pieper, Phys. Rev. Lett. **89**, 182501 (2002).
[18] R. Machleidt, F. Sammarruca, and Y. Song, Phys. Rev. C **53**, R1483 (1996).
[19] J. Carlson and V. R. Pandharipande, Nucl. Phys. **A371**, 301 (1981).
[20] J. Carlson, V. R. Pandharipande, and R. B. Wiringa, Nucl. Phys. **A401**, 59 (1983).
[21] J. Fujita and H. Miyazawa, Prog. Theor. Phys. **17**, 360 (1957).
[22] B. S. Pudliner, V. R. Pandharipande, J. Carlson, and R. B. Wiringa, Phys. Rev. Lett. **74**, 4396 (1995).
[23] R. Guardiola, in *Microscopic Quantum Many-Body Theories and Their Applications: Proceedings of a European Summer School, Held at Valencia, Spain, 8–19 September 1997*. Lecture Notes in Physics, edited by J. Navarro and A. Polls (Springer, New York, 1998), Vol. 510.
[24] L. Mitas, in *Quantum Monte Carlo Methods in Physics and Chemistry,* NATO Sci. Ser. C: Math. Phys. Sci., edited by M. P. Nightingale and C. J. Umrigar (Springer, New York, 1999), Vol. 525.
[25] S. C. Pieper, in *Microscopic Quantum Many-Body Theories and Their Applications: Proceedings of a European Summer School, Held at Valencia, Spain, 8–19 September 1997*. Lecture Notes in Physics, edited by J. Navarro and A. Polls (Springer, New York, 1998), Vol. 510.
[26] J. Carlson, in *Quantum Monte Carlo Methods in Physics and Chemistry,* NATO Sci. Ser. C: Math. Phys. Sci., edited by M. P. Nightingale and C. J. Umrigar (Springer, New York, 1999), Vol. 525.
[27] S. E. Koonin, D. J. Dean, and K. Langanke, Phys. Rep. **278**, 1 (1997).
[28] A. Sarsa, S. Fantoni, K. E. Schmidt, and F. Pederiva, Phys. Rev. C **68**, 024308 (2003).
[29] F. Pederiva, A. Sarsa, K. E. Schmidt, and S. Fantoni, Nucl. Phys. **A742**, 255 (2004).
[30] S. Gandolfi, Ph.D. thesis, University of Trento, 2007, arXiv:0712.1364 [nucl-th].
[31] P. J. Reynolds and D. M. Ceperley, J. Chem. Phys. **77**, 5593 (1982).
[32] K. E. Schmidt and M. H. Kalos, in *Applications of the Monte Carlo Method in Statistical Physics*, Topics in Current Physics, edited by K. Binder (Springer, New York, 1984), Vol. 36.
[33] J. B. Anderson, J. Chem. Phys. **65**, 4121 (1976).
[34] S. Zhang and H. Krakauer, Phys. Rev. Lett. **90**, 136401 (2003).
[35] S. Zhang, J. Carlson, and J. E. Gubernatis, Phys. Rev. Lett. **74**, 3652 (1995).
[36] S. Zhang, J. Carlson, and J. E. Gubernatis, Phys. Rev. B **55**, 7464 (1997).

[37] S. Gandolfi, F. Pederiva, S. Fantoni, and K. E. Schmidt, Phys. Rev. C **73**, 044304 (2006).
[38] S. Gandolfi, F. Pederiva, and S. a Beccara, Eur. Phys. J. A **35**, 207 (2008).
[39] J. Carlson, Phys. Rev. C **36**, 2026 (1987).
[40] G. Ortiz, D. M. Ceperley, and R. M. Martin, Phys. Rev. Lett. **71**, 2777 (1993).
[41] J. Carlson, J. E. Gubernatis, G. Ortiz, and S. Zhang, Phys. Rev. B **59**, 12788 (1999).
[42] R. B. Wiringa, S. C. Pieper, J. Carlson, and V. R. Pandharipande, Phys. Rev. C **62**, 014001 (2000).
[43] L. Colletti, F. Pederiva, E. Lipparini, and C. Umrigar, Eur. Phys. J. B **27**, 385 (2002).
[44] C. Lin, F. H. Zong, and D. M. Ceperley, Phys. Rev. E **64**, 016702 (2001).
[45] M. Baldo and C. Maieron, Phys. Rev. C **69**, 014301 (2004).
[46] S. Gandolfi, S. C. Pieper, and J. Carlson (private communication).
[47] L. Brualla, S. Fantoni, A. Sarsa, K. E. Schmidt, and S. A. Vitiello, Phys. Rev. C **67**, 065806 (2003).
[48] S. Fantoni and K. E. Schmidt, Nucl. Phys. **A690**, 456 (2001).
[49] S. Fantoni, A. Sarsa, and K. E. Schmidt, Phys. Rev. Lett. **87**, 181101 (2001).
[50] A. Akmal, V. R. Pandharipande, and D. G. Ravenhall, Phys. Rev. C **58**, 1804 (1998).
[51] O. E. Nicotra, M. Baldo, G. F. Burgio, and H. J. Schulze, Astron. Astrophys. **451**, 213 (2006).
[52] S. Gandolfi, A. Y. Illarionov, S. Fantoni, F. Pederiva, and K. E. Schmidt, Phys. Rev. Lett. **101**, 132501 (2008).
[53] A. Fabrocini, S. Fantoni, A. Y. Illarionov, and K. E. Schmidt, Phys. Rev. Lett. **95**, 192501 (2005).
[54] A. Gezerlis and J. Carlson, Phys. Rev. C **77**, 032801(R) (2008).
[55] B. Borasoy, E. Epelbaum, H. Krebs, D. Lee, and U.-G. Meissner, Eur. Phys. J. A **35**, 357 (2008).
[56] D. Lee, arXiv:0804.3501.
[57] S. C. Pieper, K. Varga, and R. B. Wiringa, Phys. Rev. C **66**, 044310 (2002).
[58] C. Pethick, D. Ravenhall, and C. Lorenz, Nucl. Phys. **A584**, 675 (1995).